Inorganic Chemistry

Article

pubs.acs.org/IC

Synthesis and Characterization of the Europium(III) Pentakis(picrate) Complexes with Imidazolium Countercations: Structural and Photoluminescence Study

Alex S. Borges,[†,⊥] José Diogo L. Dutra,[‡] Ricardo O. Freire,[‡] Renaldo T. Moura, Jr.,[§] Jeferson G. Da Silva,[†] Oscar L. Malta,[§] Maria Helena Araujo,[†] and Hermi F. Brito*[,▽]

[†]Departamento de Química, Instituto de Ciências Exatas, Universidade Federal de Minas Gerais, Belo Horizonte—MG, 31270-901, Brazil

[‡]Departamento de Química, Universidade Federal de Sergipe, 49100-000, São Cristóvão—SE, Brazil

[§]Departamento de Química Fundamental, Universidade Federal de Pernambuco, CCEN, 50590-470 Recife, PE, Brazil

[▽]Instituto de Química, Departamento de Química Fundamental, Universidade de São Paulo, Av. Prof. Lineu Prestes, 748, 05508-900, São Paulo-SP, Brazil

Supporting Information

ABSTRACT: Six new lanthanide complexes of stoichiometric formula $(C)_2[Ln(Pic)_5]$—where (C) is a imidazolium cation coming from the ionic liquids 1-butyl-3-methylimidazolium picrate (BMIm-Pic), 1-butyl-3-ethylimidazolium picrate (BEIm-Pic), and 1,3-dibutylimidazolium picrate (BBIm-Pic), and Ln is Eu(III) or Gd(III) ions—have been prepared and characterized. To the best of our knowledge, these are the first cases of Ln(III) pentakis(picrate) complexes. The crystal structures of $(BEIm)_2[Eu(Pic)_5]$ and $(BBIm)_2[Eu(Pic)_5]$ compounds were determined by single-crystal X-ray diffraction. The $[Eu(Pic)_5]^{2-}$ polyhedra have nine oxygen atoms coordinated to the Eu(III) ion, four oxygen atoms from bidentate picrate, and one oxygen atom from monodentate picrate. The structures of the Eu complexes were also calculated using the sparkle model for lanthanide complexes, allowing an analysis of intramolecular energy transfer processes in the coordination compounds. The photoluminescence properties of the Eu(III) complexes were then studied experimentally and theoretically, leading to a rationalization of their emission quantum yields.

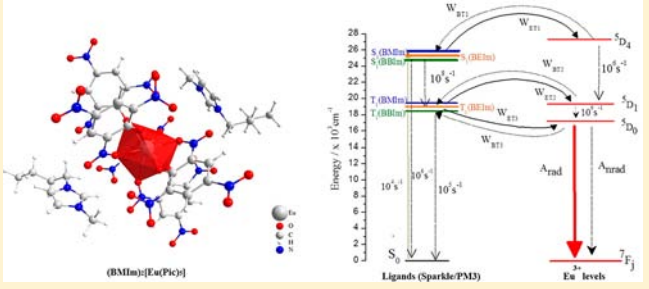

1. INTRODUCTION

There is great interest in the study of the luminescence properties of trivalent lanthanide complexes with organic ligands. Special interest lies in the possibility of designing light-conversion molecular devices (LCMDs) based on such complexes, and their applications as optical signal amplifiers, electroluminescent devices and luminescent probes in biological systems, etc.[1−4]

To obtain an efficient LCMD, it is necessary to optimize the luminescence process, which has been achieved using different organic chromophores. This sensitization process consists, initially, of the absorption of light by the ligand in the UV region, followed by a nonradiatively energy generally transferred from the triplet state (T_1) of the ligand to an excited level of the Ln(III) ion (antenna effect),[5] and, finally, the excited Ln ion decays to the ground state via photon emission in the visible region. The excitation in the ligands is much more efficient than that directly in the Ln(III) ion, because absorption coefficients of the ligands are several orders of magnitude larger than the intrinsically low molar absorption coefficients (typically 1−10 M^{-1} cm^{-1}) of Ln ions.[6−9] However, it is important to emphasize that emission by Ln(III) complexes is quenched when water or other solvent molecules, which have high-energy vibrational modes, are coordinated to the metal ion.

Therefore, the design of Ln(III) complexes with efficient photonic properties has become an important research goal, working with many different classes of ligands, such as amide,[10] sufoxides,[11] β-diketones,[3] picrates,[12] etc. Another important aspect in the design of highly luminescent materials is the efficiency of the excitation energy transfer from the ligand to the Ln(III) ion, which depends mainly on the position of the ligand's triplet state, relative to the emitting level of the metal ion (resonance condition). The former depends not only on the ligand's nature but also on the local symmetry of the metal ion.

Moreover, in the field of Ln(III) coordination compounds, the semiempirical Sparkle model can be used as an important tool in the design of new LCMDs,[13−15] since it allows the treatment of a great number of lanthanide complexes in a relatively short time. This model has been extensively applied to the calculation of ground-state geometry of these molecules. The knowledge of the

Received: August 13, 2012
Published: November 14, 2012

geometry is necessary to predict spectroscopic properties, singlet and triplet energy positions, and electronic spectra of Ln(III) complexes.[16,17] With these quantities, it is possible to build rate equations that involve the energy transfer mechanism to calculate the quantum yields for these complexes.[18]

The relationship between the metal ion and the ligands in the complex is also another important factor in designing LCMDs. The higher ratio of ligands that efficiently transfer energy to the Ln(III) ion leads to a greater probability of emission of light by the ion. It has been reported in the literature that Ln(III) complexes with a ligand-to-metal ratio of 3:1 (LnL_3, tris complex) or 4:1 (LnL_4^-, tetrakis complex).[3,19−22] In the LnL_3 anhydrous complexes, the vacant coordination positions may be occupied by additional neutral organic ligands.

Some LnL_4^- anionic complexes have been prepared combining ionic liquids (ILs) and β-diketonate to obtain new LCMDs.[19−22] Ionic liquids (ILs) are salts with melting points of <100 °C.[23−25] The cation of an IL is usually a large organic cation, such as imidazolium, pyridinium, or quaternary ammonium ions, and the anion can be inorganic or organic-like halides, BF_4^-, PF_6^-, $CF_3SO_3^-$, $(CF_3SO_2)_2N^-$, or picrate. Imidazolium ILs that contain the 1-alkyl-3-methylimidazolium cation are the most popular.

We describe herein the preparation, characterization and spectroscopic studies of six new Ln(III) pentakis(picrate) complexes that, to the best of our knowledge, are the first pentakis picrate complexes: $(BMIm)_2[Eu(Pic)_5]$ (**1**), $(BEIm)_2[Eu(Pic)_5]$ (**2**), $(BBIm)_2[Eu(Pic)_5]$ (**3**), $(BMIm)_2[Gd(Pic)_5]$ (**4**), $(BEIm)_2[Gd(Pic)_5]$ (**5**), and $(BBIm)_2[Gd(Pic)_5]$ (**6**). The Sparkle model was used to calculate the geometry of complex **1**. The X-ray crystal structures of compounds **2** and **3** are described. The electronic spectra of the ligands coordinated to the Ln(III) ion were calculated using the INDO/S−CI method.[26] Furthermore, the theoretical and experimental emission intensities of the $^5D_0 \rightarrow {}^7F_{0-4}$ transitions of the Eu(III) ion for complexes **1**−**3** were analyzed and discussed.

The experimental analysis of the Ω_2 and Ω_4 intensity parameters were made through the $^5D_0 \rightarrow {}^7F_2$ and $^5D_0 \rightarrow {}^7F_4$ transitions, using the magnetic dipole $^5D_0 \rightarrow {}^7F_1$ transition as a point of reference. The theoretical analysis of these parameters was based on the Simple Overlap Model (SOM) for the ligand field and the average energy denominator method to treat the forced electric dipole contribution to the 4*f*−4*f* intensities. The dynamic coupling mechanism was also taken into account based on the point dipole isotropic ligating atom polarizability approximation.[27]

2. EXPERIMENTAL SECTION

General Methods. All manipulations were performed under N_2 atmosphere, using standard Schlenk glassware. Reagents and solvents were purchased from commercial vendors (Aldrich, Strem Chemicals), were of the highest available purity, and were used without further purification, unless otherwise specified. Solvents used in the syntheses were dried by standing over appropriate drying agents and distilled under nitrogen (dichloromethane and ethylacetate over CaH_2 and toluene over sodium wire). 1-Methylimidazole and 1-*n*-buthylimidazole were distilled from KOH. 1-bromobutane and bromoethane were washed with concentrated H_2SO_4 and distilled from P_2O_5. $[Ln(pic)_2(H_2O)_6](pic)\cdot 6(H_2O)$ complex was prepared according to literature procedures.[28] *[CAUTION! Although we have experienced no problems in handling picrate compounds, these should be handled with great caution, because of the potential for explosion.]* The commom ILs precursors (BMIm-Br, BEIm-Br, BMIm-Br, and BMIm-Pic) were synthesized as described in the Supporting Information. The metal ions were determined by ethylenediamine tetraacetic acid (EDTA) titration using Xylenol Orange as an indicator. C, H, and N concentrations were determined using a model 2400 PerkinElmer Series 2 system. Conductivity measurements were carried out with a conductivity meter (Model HI 8033, Hanna) using 10^{-3} mol L^{-1} solutions of nitromethane at 25 °C. IR spectra were recorded on Perkin−Elmer FTIR GX instrument using KBr pellets in the 400−4000 cm^{-1} region. UV−vis absorption spectrum was recorded at room temperature with a Shimadzu Model UV-2401PC device. ^{1}H NMR spectra were recorded on a Bruker Avance DPX200 spectrometer. Values for chemical shifts are referenced to the residual solvent proton resonances in $CDCl_3$, (δ 7.24 ppm) with TMS as an internal standard. Crystal diffraction data for all compounds were collected using an Oxford-Diffraction GEMINI-Ultra diffractometer (LabCri-UFMG) using graphite-Enhance Source Mo Kα radiation (λ = 0.71073 Å) at 150(2) K. The data collection, cell refinements, and data reduction were performed using the CRYSALISPRO software.[29] The excitation and emission spectra of the Ln(III) complexes in solid state at room temperature (298 K) and liquid nitrogen temperature (77 K) were recorded at an angle of 22.5° (front face) with a spectrofluorimeter (SPEX-Fluorolog 2) with a double-grating 0.22 m monochromator (SPEX1680), and a 450-W xenon lamp as an excitation source. All spectra were recorded using a detector mode correction. The luminescence decay curves of the emitting levels were measured using a SPEX 1934D phosphorimeter accessory coupled to the spectrofluorometer. The luminescence instruments were fully controlled by a DM3000F spectroscopic computer program and the spectral intensities were automatically corrected for the photomultiplier response.

Preparation of 1-*n*-Butyl-3-ethylimidazolium Picrate (BEIm-pic). BEIm-Br (10 mmol) and potassium picrate (10 mmol) were added as solids to a mixture of deionized water (50 mL) and methanol (10 mL). The reaction mixture was stirred and refluxed for 5 h. The resultant yellow solution was then cooled to room temperature and BEIm-pic extracted with dichloromethane (100 mL). The dichloromethane solution of the picrate salt was washed three times with deionized water (100 mL each time), whereupon volatiles were removed and the product dried under vacuum at 70 °C for 24 h. The same procedure was used to prepare 1,3-dibutylimidazolium picrate (BBIm-pic).

BEIm-Pic ($C_{15}H_{19}N_5O_7$). Anal. Calcd. for $C_{15}H_{19}N_5O_7$ (381.34): C, 47.24; H, 5.02; N, 18.37%. Found: C, 46.91; H, 4.43; N, 18.04%. Mp: 66−70 °C. IR (KBr, cm^{-1}): 3143 (ν_s(H−C=C−H)), 3087 (ν_{as}(H−C=C−H)), 2964 (ν_{as}(−CH_3)), 1564, 1558 (ν_{as}(−NO_2)), 1485 (ν_{as}(C=C)), 1366, 1337 (ν_s(−NO_2)), 1269 (ν(C−O)). The main signals in ^{1}H NMR (200 MHz, $CDCl_3$, δ in ppm): δ 9.94 (1H, s, NCHN), 8,82 (2H, s, HCCNO_2CH), 7.42 (1H, m, CH_3NCHCHN), 7.38 (1H, m, CH_3NCHCHN), 4.45 (2H, m, NCH_2CH_3), 4.35 (2H, m, N$CH_2(CH_2)_2CH_3$), 1.90 (2H, m, N$CH_2CH_2CH_2CH_3$), 1.61 (3H, t, J = 7.5 Hz, N(CH_2CH_3)), 1.37 (2H, m, N$(CH_2)_2CH_2CH_3$), 0.95 (3H, t, J = 7.8 Hz, N$(CH_2)_3CH_3$). Yield = 74%.

BBIm-Pic ($C_{17}H_{23}N_5O_7$). Anal. Calcd. for $C_{17}H_{23}N_5O_7$ (409.39): C, 49.87; H, 5.66; N, 17.11%. Found: C, 50.09; H, 5.28; N, 17.01%. Mp: 55−59 °C. IR (KBr, cm^{-1}): 3111 (ν_{as}(H−C=C−H)), 1561 (ν_{as}(−NO_2)), 1363, 1334 (ν_s(−NO_2)), 1281 (ν(C−O)). The main signals in ^{1}H NMR (200 MHz, $CDCl_3$, δ in ppm): δ 9.90 (1H, s, NCHN), 8.82 (2H, s, HCCNO_2CH), 7.39 (2H, m, NCHCHN), 4.36 (4H, t, J = 7.4 Hz, $(NCH_2(CH_2)_2CH_3)_2$), 1.90 (4H, m, $(NCH_2CH_2CH_2CH_3)_2$), 1.37 (4H, m, $(N(CH_2)_2CH_2CH_3)_2$), 0.95 (6H, t, J = 7.3 Hz, $(N(CH_2)_3CH_3)_2$). Yield = 74%.

Preparation of $(BMIm)_2[Eu(Pic)_5]$ (1). A ethanol solution (10 mL) of $[Eu(pic)_2(H_2O)_6](pic)\cdot 6(H_2O)$ (1.32 g, 1.25 mmol) was added dropwise to a yellow acetonitrile solution (10 mL) of BMIm-Pic (1.01 g, 3.00 mmol). The mixture was stirred at room temperature for 5 h, after which time the solvents were removed under vacuum. A yellow solid was obtained and washed with ethanol (40 mL) and dried under vacuum. The same procedure was used to prepare $(BEIm)_2[Eu(Pic)_5]$ (**2**), $(BBIm)_2[Eu(Pic)_5]$ (**3**), $(BMIm)_2[Gd(Pic)_5]$ (**4**), $(BEIm)_2[Gd(Pic)_5]$ (**5**), and $(BBIm)_2[Gd(Pic)_5]$ (**6**).

$(BMIm)_2[Eu(Pic)_5]$ (1). Anal. Calcd. for $C_{46}H_{40}N_{19}EuO_{35}$: C, 35.17%; H, 2.57%; N, 16.94%; Eu, 9.67%. Found: C, 36.67%; H, 2.51%; N, 17.14%; Eu, 9.43%. IR (KBr, cm^{-1}): 917 (ν(CN)), 1335 and 1364

($\nu_s(NO_2)$), 1542 and 1577 ($\nu_{as}(NO_2)$), 839 ($\delta(NO_2)$), 1271 (ν(CO)), 1615 (ω(CC)), 788 (γ(CH)), 3153 (ν_s(−HC═CH−)), 3088 ($\nu_{as}(CH_3)$). Molar conductivity: 164 $cm^2\ \Omega^{-1}\ mol^{-1}$. Yield = 85%.

*(BEIm)$_2$[Eu(Pic)$_5$] (**2**).* Anal. Calcd. for $C_{48}H_{44}N_{19}EuO_{35}$: C, 36.06%; H, 2.77%; N, 16.64%; Eu 9.50%. Found: C, 35.90%; H, 2.72%; N, 16.62%; Eu, 9.80%. IR (KBr, cm^{-1}): 918 (ν(CN)), 1344 and 1364 ($\nu_s(NO_2)$), 1546 and 1578 ($\nu_{as}(NO_2)$), 844 ($\delta(NO_2)$), 1270 (ν(CO)), 1614 (ω(CC)), 788 (γ(CH)), 3148 (ν_s(−HC═CH−)), 3102 ($\nu_{as}(CH_3)$). Molar conductivity: 158 $cm^2\ \Omega^{-1}\ mol^{-1}$. Yield = 90%.

*(BBIm)$_2$[Eu(Pic)$_5$] (**3**).* Anal. Calcd. for $C_{52}H_{52}N_{19}EuO_{35}$: C, 37.74%; H, 3.17%; N, 16.23%; Eu, 9.18%. Found: C, 38.83%; H, 2.90%; N, 16.84%; Eu 9.62%. IR (KBr, cm^{-1}): 920 (ν(CN)), 1346 and 1364 ($\nu_s(NO_2)$), 1550 and 1576 ($\nu_{as}(NO_2)$), 844 ($\delta(NO_2)$), 1266 (ν(CO)), 1614 (ω(CC)), 788 (γ(CH)), 3150 (ν_s(−HC═CH−)), 3096 ($\nu_{as}(CH_3)$). Molar conductivity: 156 $cm^2\ \Omega^{-1}\ mol^{-1}$. Yield = 89%.

*(BMIm)$_2$[Gd(Pic)$_5$] (**4**).* Anal. Calcd. for $C_{46}H_{40}N_{19}GdO_{35}$: C, 35.05%; H, 2.56%; N, 16.88%; Gd 9.98%; Found: C, 35.74%; H, 2.62%; N, 16.88%; Gd, 9.68%. IR (KBr, cm^{-1}): 922 (ν(CN)), 1330 and 1364 ($\nu_s(NO_2)$), 1548 and 1575 ($\nu_{as}(NO_2)$), 828 ($\delta(NO_2)$), 1268 (ν(CO)), 1615 (ω(CC)), 788 (γ(CH)), 3153 (ν_s(−HC═CH−)), 3065 ($\nu_{as}(CH_3)$). Molar conductivity: 185 $cm^2\ \Omega^{-1}\ mol^{-1}$. Yield = 85%.

*(BEIm)$_2$[Gd(Pic)$_5$] (**5**).* Anal. Calcd. for $C_{48}H_{44}N_{19}GdO_{35}$: C, 35.94%; H, 2.76%; N, 16.59%; Eu, 9.80%. Found: C, 38.46%; H, 3.17%; N, 17.82%; Eu, 10.08%. IR (KBr, cm^{-1}): 920 (ν(CN)), 1346 and 1364 ($\nu_s(NO_2)$), 1550 and 1576 ($\nu_{as}(NO_2)$), 844 ($\delta(NO_2)$), 1266 (ν(CO)), 1616 (ω(CC)), 788 (γ(CH)), 3150 (ν_s(−HC═CH−)), 3096 ($\nu_{as}(CH_3)$). Molar conductivity: 169 $cm^2\ \Omega^{-1}\ mol^{-1}$. Yield = 90%.

*(BBIm)$_2$[Gd(Pic)$_5$] (**6**).* Anal. Calcd. for $C_{52}H_{52}N_{19}GdO_{35}$: C, 37.62%; H, 3.16%; N, 16.03%; Gd, 9.47%. Found: C, 39.08%; H, 2.95%; N, 15.90%; Gd, 9.62%. IR (KBr, cm^{-1}): 918 (ν(CN)), 1344 and 1364 ($\nu_s(NO_2)$), 1546 and 1576 ($\nu_{as}(NO_2)$), 842 ($\delta(NO_2)$), 1268 (ν(CO)), 1616 (ω(CC)), 788 (γ(CH)), 3148 (ν_s(−HC═CH−)), 3102 ($\nu_{as}(CH_3)$). Molar conductivity: 151 $cm^2\ \Omega^{-1}\ mol^{-1}$. Yield = 89%.

Component (C) in the (C)$_2$[Eu(Pic)$_5$]-prepared complexes is 1-butyl-3-methylimidazolium, (BMIm)$_2$[Eu(Pic)$_5$] (**1**); 1-butyl-3-ethylimidazolium, (BEIm)$_2$[Eu(Pic)$_5$] (**2**); or 1,3-dibutylimidazolium, (BBIm)$_2$[Eu(Pic)$_5$] (**3**) (see Scheme 1). These are the first pentakis complexes $(LnL_5)^{2-}$ with picrate ligand.

Scheme 1. Structural Representation of the Eu(III)-Picrate Complexes with the Imidazolium Countercations: 1-Butyl-3-methylimidazol, (BMIm)$_2$[Eu(Pic)$_5$] (1); 1-Butyl-3-ethylimidazolium, (BEIm)$_2$[Eu(Pic)$_5$] (2); and 1,3-Dibutylimidazolium, (BBIm)$_2$[Eu(Pic)$_5$] (3)

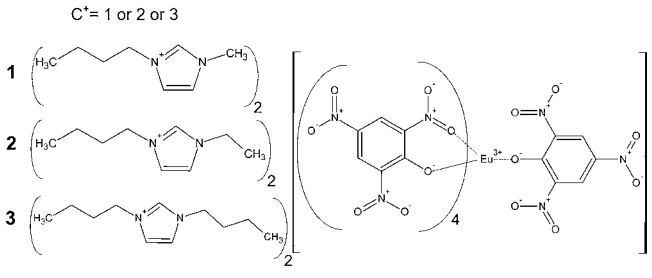

X-ray Crystallography. The crystal structures of complexes **2** and **3** were investigated using single-crystal X-ray diffraction (XRD). Semi-empirical from equivalents absorption correction method was applied. The structure was solved using the SHELXS-97 program.[30] Full-matrix least-squares refinement procedure on F^2 with anisotropic thermal parameters was carried on using SHELXL-97 program.[30] Positional and anisotropic atomic displacement parameters were refined for all non-hydrogen atoms. Hydrogen atoms were placed geometrically and the positional parameters were refined using a riding model. The data presented in Tables 1, 2, and 4 were compiled using WINGX and PLATON software suites.[31,32] Crystal and structure refinement data are summarized in Table 1.

3. THEORETICAL DETAILS

Geometry Optimization. Initially, the crystallographic structures of compounds **2** and **3** were used to evaluate which computational methodology, between Sparkle/AM1, Sparkle/PM3 and Sparkle/PM6, would be more appropriated to study the series of Eu(III) complexes. Based on this analysis, the ground-state geometry of compounds **1**, **2**, and **3** were calculated with the Sparkle/PM3 model,[14] implemented in the MOPAC 2009 package.[33] The MOPAC keywords used were as follows: SPARKLE, PRECISE, GNORM = 0.25, SCFCRT = 1.D-10 (in order to increase the SCF convergence criterion), and XYZ (the geometry optimizations were performed in Cartesian coordinates).

The optimized geometries were used as input to calculate the ligand singlet and triplet excited states in the Eu complexes using configuration interaction with single excitations (CIS), based on the intermediate neglect of the differential overlap/spectroscopic (INDO/S) technique implemented in the ZINDO package.[34,35] We have used a point charge of +3*e* to represent the Eu(III) ion.

The Judd−Ofelt Intensity Parameters. The forced electric dipole contribution to the 4*f*−4*f* intensities is described by the Judd−Ofelt theory.[36,37] The intensity parameters (IP) Ω_λ (λ = 2, 4, and 6) are defined by

$$\Omega_\lambda = (2\lambda + 1)\sum_{t,p}\frac{|B_{\lambda tp}|^2}{(2t+1)} \quad (1)$$

$$B_{\lambda tp} = B^{ed}_{\lambda tp} + B^{dc}_{\lambda tp} \quad (2)$$

where

$$B^{ed}_{\lambda tp} = \frac{2}{\Delta E}\langle r^{t+1}\rangle\theta(t,p)\gamma^t_p \quad (3)$$

and

$$B^{dc}_{\lambda tp} = -\left[\frac{(\lambda+1)(2\lambda+3)}{2\lambda+1}\right]^{1/2}\langle r^\lambda\rangle(1-\sigma_\lambda) \times \langle f\|C^{(\lambda)}\|f\rangle\Gamma^t_p\delta_{t,\lambda+1} \quad (4)$$

The first and second terms in eq 2 correspond to the forced electric dipole ("ed") and dynamic coupling ("dc") mechanisms, respectively. The quantities γ^t_p (odd-rank ligand field parameters) and Γ^t_p (ligating atom polarizability-dependent terms) in eqs 3 and 4, respectively, contain a sum over the ligating atoms. The nature of the chemical environment and structural aspects in the first coordination sphere of the Ln ion are precisely taken into account in this sum. In eq 3, the numerical factor $\theta(t, \lambda)$ is a function of the lanthanide ion; in eq 4, the quantities $\langle r^\lambda\rangle$, $(1-\sigma_\lambda)$, and $\langle f\|C^{(\lambda)}\|f\rangle$ are a radial integral, a shielding factor, and a one-electron reduced-matrix element, respectively.[38]

The experimental intensity parameters were calculated from the coefficients of spontaneous emission, according to the following expression:

$$\Omega_\lambda = \frac{3\hbar c^3 A_{0\lambda}}{4e^2\omega^3\chi\langle {}^7F_\lambda\|U^{(\lambda)}\|{}^5D_0\rangle^2} \quad (5)$$

where χ is the Lorentz local field correction term, given by $\chi = n(n^2+2)^2/9$ and $\langle {}^7F_\lambda\|U^{(\lambda)}\|{}^5D_0\rangle^2$ is a squared reduced matrix element whose value is 0.0032 and 0.0023 for the ${}^5D_0 \rightarrow {}^7F_2$ and ${}^5D_0 \rightarrow {}^7F_4$ transitions, respectively.[39] The index of refraction (n) has been assumed to be equal to 1.5.

dx.doi.org/10.1021/ic301776n | Inorg. Chem. 2012, 51, 12867−12878

Table 1. Crystal Data and Structure Refinement for the $(BEIm)_2[Eu(Pic)_5]$ (2) and $(BBIm)_2[Eu(Pic)_5]$ (3) Complexes

crystal data	2	3
empirical formula	$C_{48}H_{44}EuN_{19}O_{35}$	$C_{52}H_{52}EuN_{19}O_{35}$
formula weight	1598.98	1655.09
crystal system	triclinic	triclinic
space group	$P\bar{1}$	$P\bar{1}$
unit-cell dimensions		
a (Å)	11.075(5)	11.4030(3)
b (Å)	12.458(5)	16.7616(5)
c (Å)	23.229(5)	18.1245(5)
α (°)	75.927(5)	103.359(2)
β (°)	76.995(5)	92.328(2)
γ (°)	88.684(5)	104.577(2)
volume, V (Å^3)	3027.3(19)	3243.96(16)
Z	2	2
density (calc.) (Mg m^{-3})	1.754	1.694
absorption coefficient (mm^{-1})	1.155	1.081
$F(000)$	1616	1680
crystal size (mm^3)	0.23 × 0.11 × 0.03	0.28 × 0.14 × 0.06
θ range for data coll. (°)	2.64−26.37	2.75−26.37
index ranges	$-13 \le h \le 13, -15 \le k \le 15, -29 \le l \le 29$	$-14 \le h \le 14, -20 \le k \le 20, -22 \le l \le 22$
reflection collected	62150	60043
independent reflections	12373 [R(int) = 0.0772]	13251 [R(int) = 0.0632]
completeness (%)	99.9 (to 26.37°)	99.9 (to 26.37°)
max. and min. transmission	0.9662 and 0.7770	0.9380 and 0.7516
data/restraints/parameters	12373/0/928	13251/0/964
goodness of fit on F^2	1.039	1.059
R indices (all data)	$R1$ = 0.0396, $wR2$ = 0.0786	$R1$ = 0.0329, $wR2$ = 0.0600
final R indices [$I > 2\sigma(I)$]	$R1$ = 0.0530, $wR2$ = 0.0831	$R1$ = 0.0445, $wR2$ = 0.0644
largest peak and hole (Å^{-3})	1.289 and −1.171	0.951 and −0.497

In eq 5, $A_{0\lambda}$ (λ = 2 and 4) represents spontaneous emission coefficients, calculated by taking the magnetic dipole transition $^5D_0 \rightarrow {}^7F_1$ as the reference, once this transition is practically insensitive to the chemical environment around the Eu ion. The following expression was used:

$$A_{0\lambda} = A_{01}\left(\frac{S_{0\lambda}}{S_{01}}\right)\left(\frac{\nu_{01}}{\nu_{0\lambda}}\right) \tag{6}$$

where S_{01} and $S_{0\lambda}$ are the areas under the curves of the $^5D_0 \rightarrow {}^7F_1$ and $^5D_0 \rightarrow {}^7F_\lambda$ transitions, with ν_{01} and $\nu_{0\lambda}$ being their energy barycenters, respectively. The coefficient of spontaneous emission in eq 6 (A_{01}) is given by the expression $A_{01} = 0.31 \times 10^{11}(n)^3(\nu_{01})^3$, leading to an estimated value of ∼50 s^{-1}.[40]

As mentioned above, the theoretical intensity parameters were calculated using the spherical coordinates obtained from the Sparkle/PM3 coordination polyhedron of the Eu(III) complexes and eqs 1−4, with the system of coordinates centered at the Eu(III) ion. In this procedure, the charge factors (g) that appear in the ligand field parameters γ_p^t and the ligating atom polarizabilities (α) have been treated as variables within ranges of physically acceptable values. In the present case, both g and α were separated into two groups: one belonging to the oxygen unidentate of the picrate ligand and the other one belonging to the oxygen bidentate of the picrate ligand.

Intramolecular Energy Transfer and Emission Quantum Yields. The intramolecular energy transfer rates were calculated from the approach developed by Malta et al.[41,42] In this approach, the transfer rates (W_{ET}) are expressed in terms of a sum,

$$W_{ET} = W_{ET}^{mp} + W_{ET}^{ex}$$

where W_{ET}^{mp} is the transfer rate of the multipolar,

$$W_{ET}^{mp} = \frac{2\pi}{\hbar}\frac{e^2 S_L}{(2J+1)G}F\sum_\lambda\left(\frac{2(1-\sigma_1)^2\Omega_\lambda^{ed}}{{R_L}^6} + \gamma_\lambda\right) \times \langle \psi' J' \| U^{(\lambda)} \| \psi J \rangle^2 \tag{7}$$

and W_{ET}^{ex} is the transfer rate of exchange,

$$W_{ET}^{ex} = \frac{8\pi}{3\hbar}\left[\frac{e^2\langle 4f|L\rangle^4}{(2J+1){R_L}^4}\right]F\left\langle \psi' J' \| U^{(\lambda)} \| \psi J \right\rangle^2 \times \sum_m |\langle \varphi | \sum_k \mu_z(k) s_m(k) | \varphi' \rangle|^2 \tag{8}$$

At this point, it should be emphasized that shielding effects due to the filled 5s and 5p subshells have been appropriately taken into account in eq 7, and an effective exchange Hamiltonian[41] has been used in eq 8. The first and second terms in the parentheses in the righthand side (rhs) of eq 7 correspond to the dipole−dipole and dipole−2^λ pole interactions. The Ω_λ^{ed} parameters are the forced electric dipole contribution to the $4f$−$4f$ intensity parameters, J is the lanthanide ion total angular momentum, ψ specifies a given $4f$ spectroscopic term, S_L is the dipole strength of the ligand transition involved in the transfer process, and the quantities $\langle \psi' J' \| U^{(\lambda)} \| \psi J \rangle$ are reduced matrix elements of the same type as those appearing in eq 5. In eq 8, S is the total spin operator of the Ln ion, μ_z the z component of the electric dipole operator, and s_m (m = 0, ±1) a spherical component of the spin operator, both for the ligand electrons, and $\langle 4f|L\rangle$ is the total overlap integral between the $4f$ orbital and the ligand wave functions involved in the transfer process.[43] The quantities γ_λ and F are, respectively, given by

dx.doi.org/10.1021/ic301776n | Inorg. Chem. 2012, 51, 12867−12878

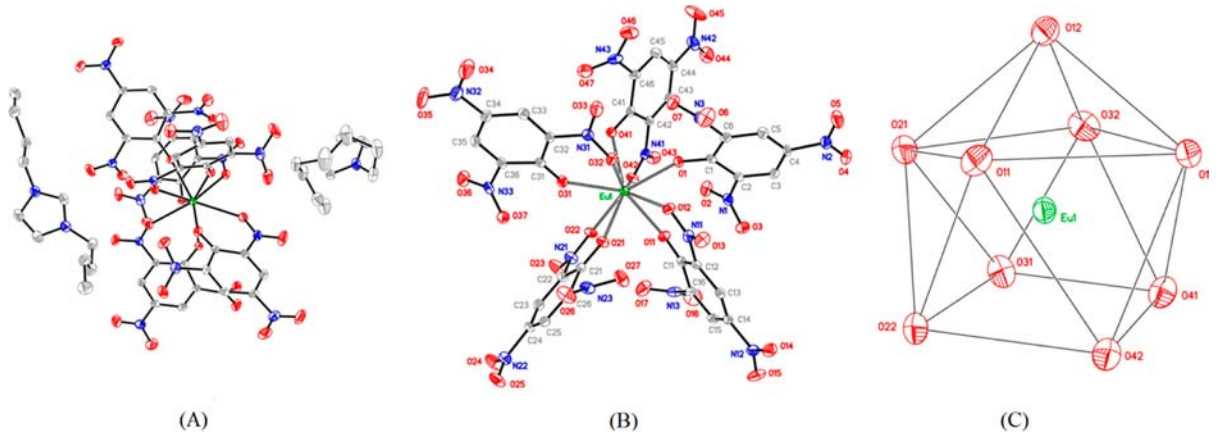

Figure 1. (A) Molecular structure of $(BBIm)_2[Eu(Pic)_5]$ (**3**) at 50% probability level. (B) Detail of molecular structure of $[Eu(Pic)_5]^{2-}$ complex with atom numbering scheme in a new projection that favors the visualization of the picrate ligands. All the H atoms have been omitted for the sake of clarity. (C) Coordination polyhedron of the Eu(III) ion in $(BEIm)_2[Eu(Pic)_5]$ (**2**).

$$\gamma_\lambda = (\lambda + 1)\frac{\langle r^\lambda\rangle^2}{(R_L{}^{\lambda+2})^2}\langle 3\|C^{(\lambda)}\|3\rangle^2(1-\sigma_\lambda)^2 \tag{9}$$

and

$$F = \frac{1}{\hbar\gamma_\lambda}\sqrt{\frac{\ln 2}{\pi}}\exp\left[-\left(\frac{\Delta}{\hbar\gamma_\lambda}\right)\right]^2 \ln 2 \tag{10}$$

where $\langle 3\|C^{(\lambda)}\|3\rangle$ is a reduced matrix element of the Racah tensor operator $C^{(\lambda)}$, the σ terms are screening factors due to the filled 5s and 5p subshells of the Eu(III) ion and $\langle r^\lambda\rangle$ is the radial expectation value of r^λ for 4*f* electrons. Typical values of the quantities appearing in eq 9 show that $\gamma_6 \ll \gamma_4 \ll \gamma_2$.

From the above equations, the following selection rules are derived: $J + J' \geq \lambda \geq |J - J'|$, for the multipolar mechanism, and $\Delta J = 0, \pm 1$ for the exchange mechanism. In both cases, $J' = J = 0$ is excluded. From the ligand side, the selection rules can be derived from the electric dipole strength S_L and the matrix element of the coupled operators μ_z and s_m in eq 8.

An appropriate system of rate equations is used to describe the kinetics of the 4*f*−4*f* luminescence in terms of the level populations N_i.[40] The general form of these equations is given by

$$\frac{dN_l}{dt} = -\left(\sum_i P_{il}\right)N_l + \sum_j P_{lj}N_j \tag{11}$$

where the sum over *i* and *j* excludes the state *l*, P_{il} stands for a transition or transfer rate starting from state *l*, and P_{lj} stands for a transition or transfer rate ending up in this state. In the steady-state regime, all of the dN_l/dt are set equal to zero. The theoretical emission quantum yield (q_{theo}) is calculated using the steady-state populations, according to

$$q_{theo} = \frac{A_{rad}N(^5D_0)}{\Phi_0 N(S_0)} \tag{12}$$

where A_{rad} is the total radiative emission rate from the $^5D_0$ level, $N(^5D_0)$ its steady-state population, and Φ_0 the absorption rate from the ligand singlet ground state S_0, with steady-state population $N(S_0)$, to the singlet ligand excited state S_1.

An important aspect to be emphasized is that the intramolecular energy transfer selection rules associated with the $^5D_0$ and $^5D_1$ levels of the Eu(III) ion, have been described in detail previously in the literature.[44] According to these rules, energy transfer to the $^5D_0$ level, with the Eu(III) ion being initially in the $^7F_0$ ground state, by the exchange mechanism, is forbidden. Besides, this energy transfer process is also forbidden by the dipole−dipole and dipole−multipole mechanisms, as long as the *J*-mixing effects, which are small, are neglected. The interpretation of our emission quantum yield results has taken into account these selection rules.

4. RESULTS AND DISCUSSION

Characterization of the Complexes. Analytical data indicate that the Eu(III) and Gd(III) complexes have a stoichiometry formula of $C_2[Ln(pic)_5]$, where C = BMIm, BEIm, BBIm. All the complexes are soluble in dimethylformamide (DMF), dimethylsulfoxide (DMSO), tetrahydrofuran (THF), acetonitrile, acetone, and nitromethane, but partially soluble in ethanol and chloroform. The complexes are also stable in air and moisture for a long period. The molar conductance of the picrate complexes in nitromethane indicates that all of the complexes act as dielectrolytes,[45] implying that all picrate groups are in the coordination sphere.

The absorption band assigned to the OH out-of-plane bending vibration of the free HPic at 1155 cm^{-1} disappears in the infrared (IR) spectra (not shown) of the complexes, indicating that the H atom of the OH group is replaced by Ln(III) ion. The vibration ν(C−O) at 1262 cm^{-1} is shifted toward higher wavenumbers by ca. 5−10 cm^{-1} in the complexes. This is due to the substitution of the hydrogen atom of the OH group by the lanthanide ion upon coordination, increasing the π-bond character in the C−O bond. The free HPic has $\nu_{as}(NO_2)$ and $\nu_s(NO_2)$ at 1558 and 1343 cm^{-1}, respectively, which split into two bands at ca. 1581, 1542 cm^{-1} and 1361, 1331 cm^{-1}, respectively, in the complexes. These results indicate that they are coordinated, at least in part, as bidentate ligands through the phenolic oxygen and one oxygen of a nitro group.[46] All IR spectral profiles of the complexes are similar.

X-ray Crystallography and the Sparkle Model. Complexes **2** and **3** crystallize in a triclinic system with space group $P\bar{1}$. The asymmetric unit of the compounds contains one $[Eu(Pic)_5]^{2-}$ anionic complex (common to both compounds and identical with respect to the coordination form of the ligands) and two 1-butyl-3-ethylimidazolium (BEIm) or two 1-butyl-3-butylimidazolium (BBIm) cations for **2** and **3**, respectively.

dx.doi.org/10.1021/ic301776n | Inorg. Chem. 2012, 51, 12867−12878

Table 2. Nonclassical Hydrogen Bonds Geometry for Complexes 2 and 3

D−H···A	symmetry transformations[a]	d(D−H) (Å)	d(H···A) (Å)	d(D···A) (Å)	∠(DHA) (°)
		$(BEIm)_2[Eu(Pic)_5]$ (**2**)			
C104—H04B···O33		0.99	2.54	3.473(6)	157
C108—H08B···O24	$-1 + x, 1 + y, z$	0.99	2.37	3.219(6)	144
C13—H13···O25	$1 - x, 1 - y, 1 - z$	0.95	2.47	3.389(5)	163
C109—H09C···O15	$-x, -y, 1 - z$	0.98	2.59	3265(6)	126
C114—H14A···O37	$-1 + x, -1 + y, z$	0.99	2.48	3.427(7)	159
C115—H15A···O23	$-1 + x, -1 + y, z$	0.99	2.57	3.457(10)	149
C117—H17B···O33	$-1 + x, y, z$	0.98	2.59	3.540(7)	163
C118—H18B···O46		0.99	2.49	3.279(6)	136
C101—H101···O13		0.95	2.42	3.151(5)	134
C101—H101···O25	$1 - x, 1 - y, 1 - z$	0.95	2.43	3.288(5)	151
C103—H103···O2	$x, 1 + y, z$	0.95	2.37	3.312(5)	170
C111—H111···O6	$x, -1 + y, z$	0.95	2.36	3.221(5)	151
C103—H113···O47	$1 - x, 1 - y, z$	0.95	2.58	3.344(5)	138
		$(BBIm)_2[Eu(Pic)_5]$ (**3**)			
C104—H04A···O15	$1 - x, 1 - y, 1 - z$	0.99	2.53	3.237(4)	128
C104—H04B···O46	$1 - x, -y, 1 - z$	0.99	2.56	3.483(4)	155
C105—H05B···O33	$1 - x, -y, 1 - z$	0.99	2.53	3.229(4)	128
C107—H07C···O5		0.98	2.49	3.318(4)	143
C101—H101···O13		0.95	2.48	3.322(3)	148
C102—H102···O7	$1 - x, -y, 1 - z$	0.95	2.58	3.278(4)	131
C103—H103...O34	$2 - x, -y - 1, -z$	0.95	2.58	3.278(4)	131
C201—H201···O17		0.95	2.58	3.110(4)	116
C202—H202···O2	$1 - x, 1 - y, z$	0.95	2.41	3.355(4)	173
C203—H203···O16	$1 - x, -y, 1 - z$	0.95	2.34	3.251(4)	161

[a]Symmetry transformations used to generate equivalent atoms.

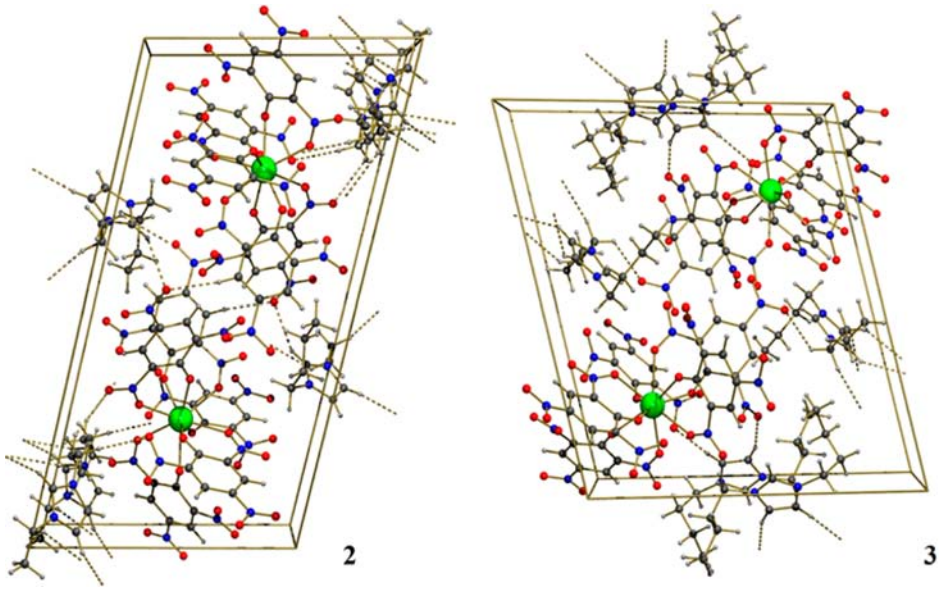

Figure 2. Views of the crystal packing of compounds **2** and **3** along the *x*-axis. The intermolecular interactions are indicated by dashed lines.

Figure 1A shows the molecular structure of $(BBIm)_2[Eu(Pic)_5]$ (**3**).

As can be seen in Figure 1B, the Eu(III) ion is nine-coordinated by O atoms of five picrate anions: four bidentade picrates via phenolic oxygen atom and one oxygen of the nitro group in each ligand, and one monodentade picrate via phenolic oxygen atom. The coordination geometry of the Eu(III) center can be described as a distorted monocapped square antiprism with the atoms O22, O31, O41, O42 on the bottom square, the atoms O1, O11, O21, O32 on the top square, and the atom O12 capping the latter (Figure 1C). The C_{4V} point group should reflect the symmetry of the complex, considering the geometry observed in the coordination polyhedron (Figure 1C).

Several geometric parameters to quantify the deformation of the coordination polyhedra, introduced by Balic-Zunic and Makovicky and implemented in the IVTON program are given.[47,48] These parameters are calculated, with respect to the centroid of the coordination polyhedron, which is the point in the coordination polyhedron where the variance of squares of distances to ligands is minimum. These parameters are the

dx.doi.org/10.1021/ic301776n | *Inorg. Chem.* 2012, 51, 12867−12878

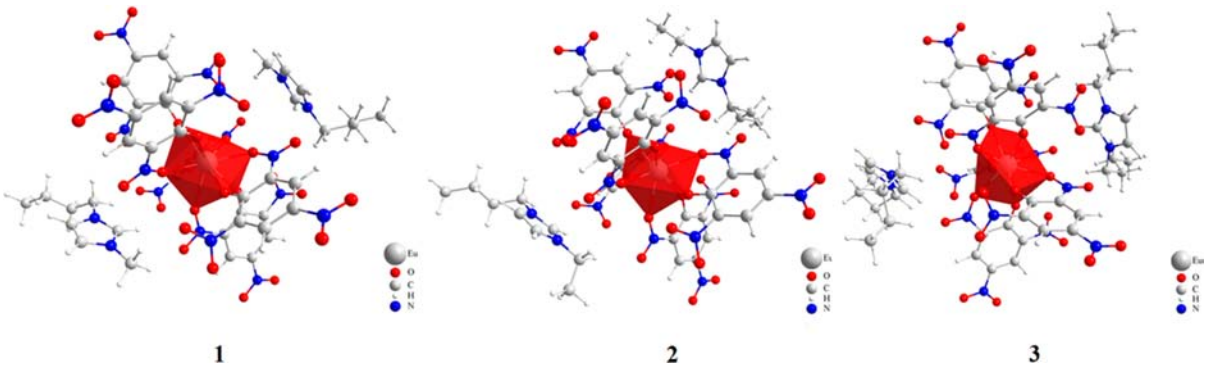

Figure 3. Calculated ground-state geometries, using the Sparkle/PM3 model, for complexes **1**, **2**, and **3**.

central atom-centroid distance (Δ), 0.026 Å in **2** and 0.034 Å in **3**, the average distance from the centroid to the ligands (r), 2.418 Å in **2** and 2.419 Å in **3**, and the "sphericity" ($1 - \sigma_r/r$) is 0.9608 in **2** and 0.9537 in **3** (σ_r is the standard deviation of the distances from the centroid to the ligands). It is noteworthy to mention that the parameters obtained for compounds **2** and **3** indicate a close similarity between these anionic complexes.

Intermolecular interactions involving the cationic species are responsible for the stability of the charge in the structure, as well as to promote the formation of hydrogen bonds with the coordinated picrate groups (Table 2). These C−H···O interactions play an important role in the crystal packing of the complexes, as can be seen in Figure 2.

The semiempirical Sparkle Model was used to calculate the structures of Eu(III) complexes **1**, **2**, and **3**. Although the three models Sparkle/AM1, Sparkle/PM3, and Sparkle/PM6 have shown similar accuracy, the semiempirical AM1, PM3, and PM6 methods present differences in the prediction of the organic part in lanthanide complexes.[13−15] For this reason, we compare the calculated structures using all versions of the Sparkle Model predictions with the crystallographic ones. The results indicate that the Sparkle/PM6 model is not suitable, because the calculated structures present a coordination number different from that given by the crystallographic structure. In the Sparkle/PM6 structure, all five picrate ligands present a bidentate coordination mode, whereas in the crystallographic structures, one of these five ligands presents a monodentate coordination mode. This problem does not occur with the Sparkle/AM1 and Sparkle/PM3 models.

Although the Sparkle/AM1 structure reproduces the Eu−O distances more accurately, both models present a similar unsigned mean error (UME) for the Eu−O distances. The UME values obtained with the Sparkle/AM1 and Sparkle/PM3 models were 0.073 and 0.096 Å, respectively. However, when all distances of the coordination polyhedron are considered, the Sparkle/PM3 model presents a UME value that is 21% smaller than that of the Sparkle/AM1. This fact indicates that the O−Eu(III)−O angles are calculated with greater accuracy by the Sparkle/PM3 model.

Figure 3 shows the Sparkle/PM3 optimized molecular structures of the three different complexes studied in the present work. Spherical atomic coordinates for the Sparkle/PM3 coordination polyhedra are summarized in Table 3. The crystallographic and theoretical bond distances and selected angles around the Eu(III) ion for the compounds are shown in Table 4.

The crystallographic average Eu−O bond lengths are 2.42(10) Å in **2** and 2.42(11) Å in **3**, whereas the Sparkle/PM3 average is 2.46(2) Å (for **2** and **3**). These values are consistent with the average observed in the crystal structures of the nine-coordinated EuO_n compounds (2.43(9) Å).[49] However, from the crystallographic data, the Eu−O distances to the nitro groups, which are in the range of 2.295−2.361 Å, are shorter than the Eu−O distances to the phenolato groups, which are in the range of 2.430(17)−2.636(18) Å. These values do not change when the

Table 3. Spherical Atomic Coordinates for the Sparkle/PM3 Coordination Polyhedron, Charge Factors (g), and the Polarizability (α) of the Coordinated Ligating Atoms for Complexes 1, 2, and 3

	Spherical Coordinates				
compound	R (Å)	θ (°)	ϕ (°)	g	α (Å^3)
$(BMIm)_2[Eu(Pic)_5]$, **1**					
O (monodentate)	2.4535	83.9004	344.8131	1.66	1.42
	2.4640	20.7500	291.3273	0.07	5.90
	2.4697	45.0451	61.9672	0.07	5.90
	2.4673	58.3408	167.6467	0.07	5.90
O (bidentate)	2.4716	82.0793	227.6074	0.07	5.90
	2.4676	136.4844	171.5151	0.07	5.90
	2.4758	103.2414	111.2200	0.07	5.90
	2.4671	141.1587	36.2626	0.07	5.90
	2.4744	139.8563	292.2950	0.07	5.90
$(BEIm)_2[Eu(Pic)_5]$, **2**					
O (monodentate)	2.4594	85.3892	342.5038	1.66	1.41
	2.4638	19.5094	298.9761	0.07	5.90
	2.4676	48.0103	61.2130	0.07	5.90
	2.4641	58.4639	174.1708	0.07	5.90
O (bidentate)	2.4678	83.5272	233.4437	0.07	5.90
	2.4665	137.0276	172.0685	0.07	5.90
	2.4727	102.0309	113.5100	0.07	5.90
	2.4708	140.7977	37.6382	0.07	5.90
	2.4777	139.6038	293.9408	0.07	5.90
$(BBIm)_2[Eu(Pic)_5]$, **3**					
O (monodentate)	2.4546	87.2539	177.1665	0.66	4.78
	2.4655	122.5652	328.6584	0.07	5.90
	2.4742	64.2857	312.4238	0.07	5.90
	2.4677	72.5814	29.3347	0.07	5.90
	2.4744	124.0575	62.4199	0.07	5.90
O (bidentate)	2.4657	64.5257	105.9369	0.07	5.90
	2.4694	9.0682	163.9353	0.07	5.90
	2.4684	100.4828	249.6164	0.07	5.90
	2.4715	154.0715	209.1267	0.07	5.90

dx.doi.org/10.1021/ic301776n | Inorg. Chem. 2012, 51, 12867−12878

Table 4. Crystallographic and Theoretical Values Obtained for Selected Bonds Lengths and Angles for Compounds 2 and 3

	$(BEIm)_2[Eu(Pic)_5]$, **2**		$(BBIm)_2[Eu(Pic)_5]$, **3**	
	crystallographic	Sparkle/PM3	crystallographic	Sparkle/PM3
		Bond Lengths (Å)		
Eu1−O1	2.345(2)	2.459	2.321(16)	2.455
Eu1−O11	2.348(2)	2.471	2.323(16)	2.466
Eu1−O12	2.555(2)	2.478	2.636(18)	2.469
Eu1−O21	2.295(2)	2.467	2.323(17)	2.468
Eu1−O22	2.487(2)	2.473	2.526(17)	2.474
Eu1−O31	2.354(2)	2.464	2.354(16)	2.466
Eu1−O32	2.484(2)	2.468	2.430(17)	2.474
Eu1−O41	2.361(2)	2.464	2.359(16)	2.468
Eu1−O42	2.533(2)	2.468	2.506(18)	2.472
	$(BEIm)_2[Eu(Pic)_5]$, **2**		$(BBIm)_2[Eu(Pic)_5]$, **3**	
	crystallographic	Sparkle/PM3	crystallographic	Sparkle/PM3
		Bond Angles (deg)		
O11−Eu1−O12	67.15(7)	60.45	65.93(6)	59.99
O21−Eu1−O22	68.60(7)	59.98	67.45(6)	60.35
O31−Eu1−O32	67.03(8)	60.55	68.91(6)	60.30
O41−Eu1−O42	65.85(7)	60.12	65.95(6)	60.62
O1−Eu1−O11	79.67(8)	72.67	76.77(6)	71.89
O1−Eu1−O12	67.07(7)	68.51	67.74(6)	78.43
O1−Eu1−O21	135.24(8)	136.78	134.73(6)	142.41
O1−Eu1−O22	139.17(7)	131.02	136.17(6)	111.92
O1−Eu1−O31	139.80(8)	142.18	142.49(6)	139.95
O1−Eu1−O32	88.12(8)	108.32	89.20(6)	128.20
O1−Eu1−O41	73.56(8)	71.51	73.60(6)	73.29
O1−Eu1−O42	73.60(7)	78.53	74.86(6)	70.88
O11−Eu1−O21	74.98(8)	74.61	75.12(6)	70.83
O11−Eu1−O22	77.00(8)	71.79	75.41(6)	72.45
O11−Eu1−O31	140.47(8)	142.78	140.56(6)	142.23
O11−Eu1−O32	131.31(7)	133.76	130.60(6)	122.78
O11−Eu1−O41	140.29(7)	139.66	141.01(6)	142.51
O11−Eu1−O42	78.86(7)	95.04	82.32(6)	118.48
O12−Eu1−O21	69.25(7)	71.09	68.63(6)	79.05
O12−Eu1−O22	130.02(7)	118.36	127.05(5)	125.39
O12−Eu1−O31	122.09(8)	132.27	122.94(6)	131.27
O12−Eu1−O32	64.68(7)	76.63	64.91(5)	72.10
O12−Eu1−O41	124.65(7)	120.15	122.50(6)	99.67
O12−Eu1−O42	131.36(7)	143.24	135.08(5)	147.09
O21−Eu1−O31	74.20(8)	78.59	74.36(6)	76.54
O21−Eu1−O32	81.93(8)	76.00	83.05(6)	71.06
O21−Eu1−O41	143.67(8)	145.73	143.61(6)	140.37
O21−Eu1−O42	134.25(7)	132.06	134.10(6)	133.35
O22−Eu1−O31	69.07(8)	72.58	70.16(6)	75.19
O22−Eu1−O32	132.15(7)	120.56	134.49(6)	119.88
O22−Eu1−O41	105.24(7)	121.44	110.38(6)	134.94
O22−Eu1−O42	69.34(7)	72.23	68.41(5)	78.41
O31−Eu1−O41	70.43(8)	70.70	71.25(6)	75.20
O31−Eu1−O42	106.36(8)	84.10	101.85(6)	72.40
O32−Eu1−O41	77.01(8)	75.90	73.89(6)	70.98
O32−Eu1−O42	141.81(7)	131.02	139.47(6)	118.74

structures are calculated using the Sparkle/PM3 model, and the analyses of the angle values indicate that the Sparkle/PM3 results are in good agreement with the crystallographic ones.

Considering these bond distances and the coordination polyhedron around the Eu(III) ions, we can suggest a lowering of the point symmetry from C_{4V} to C_1, as indeed indicated by the crystallographic data.

Absorption Spectra. Theoretical and experimental UV−vis absorption spectra of the ligands in the Eu(III) complexes are depicted in Figure 4. The experimental absorption spectra of the three complexes show a slight difference in peak positions, with a maximum displacement of 14 nm. These experimental spectra display a shoulder in the region of lower energy (higher wavelength), which suggests a ligand-to-metal charge-transfer (LMCT) state. Both the absorption and excitation spectra (see Figures 4 and 5) penetrate well in the visible region, which explains the yellow color of the compounds and confirms the absorption by picrate ligands ($S_0 \rightarrow S^*$ transition), and they

dx.doi.org/10.1021/ic301776n | Inorg. Chem. 2012, 51, 12867−12878

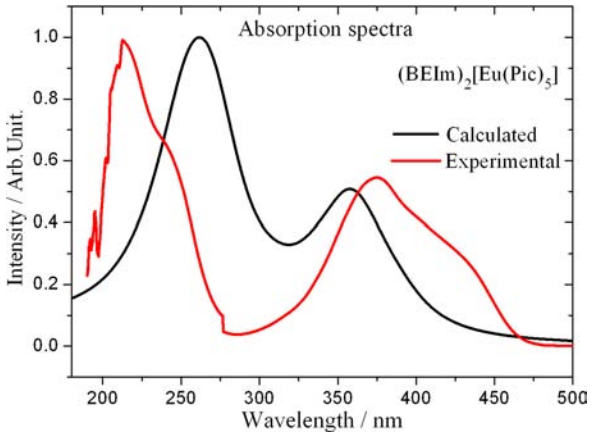

Figure 4. Absorption spectra of $(BEIm)_2[Eu(Pic)_5]$ (**2**), showing experimental data (recorded in acetonitrile solution) and theoretical prediction.

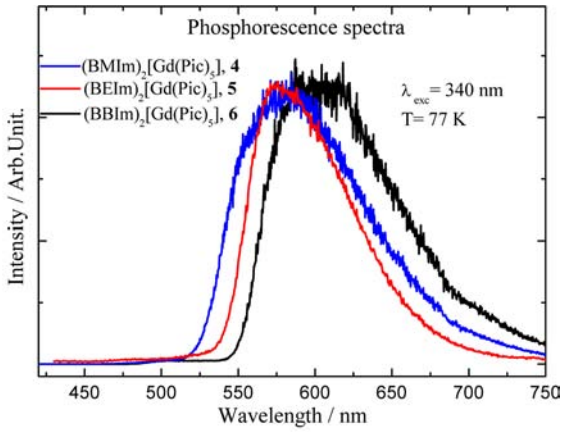

Figure 5. Phosphorescence spectra of complexes **4**, **5**, and **6** recorded at 77 K.

indicate that the energy transfer to the Eu(III) ion also is realized. However, the theoretical absorption spectra, calculated for the complexes, do not exhibit any significant difference.

The results suggest that the change of countercations affect slightly the R_L values (see Table 5). The R_L parameter is the distance from the donor state located at the organic ligand to the lanthanide ion. The change in the R_L quantities considerably influences the energy transfer and back-transfer rates.

Table 5. Experimental and Calculated Ligand Excited State Energies and R_L Values for Complexes 1−3

states		1	2	3
Singlet	Calc. (cm^{-1})	25594.2	25502.0	25384.6
	R_L (Å)	5.8327	5.1614	5.8835
	Exp. (cm^{-1})	26178	26709	25773
Triplet	Calc. (cm^{-1})	19242.3	18913.8	18449.5
	R_L (Å)	4.3432	4.5314	3.9201
	Exp. (cm^{-1})	19512	19065	18504

Experimental and Theoretical Photoluminescence Study. From the phosphorescence spectra of the Gd(III) complexes, it was possible to find the positions of the first triplet excited electronic states (T_1) of the picrate ligands. The emission spectra were recorded at 77 K, under excitation at 370 nm. The T_1 state energy was determined from the shortest wavelength corresponding to the 0−0 phonon transition at ~19 512, 19 065, and 18 504 cm^{-1} for the complexes with countercation $BMIm^+$ (**4**), $BEIm^+$ (**5**), and $BBIm^+$ (**6**), respectively (see Figure 5).

The excitation spectra of complexes **1**, **2**, and **3** recorded at 77 K are shown in Figure 6. All the excitation spectra recorded in the range of 260−600 nm, monitored at the $^5D_0 \rightarrow {}^7F_2$ hypersensitive transition at 616 nm, display a large broad band ascribed to the excited states of the ligand with three components peaking at ~290, 370, and 470 nm, corresponding to $S_0 \rightarrow S^*$ transitions and possibly an LMCT state. The energy and full width at half-maximum (fwhm) of the broad band components are different for each complex, showing that the countercation (C) present in the $(C)_2[Eu(Pic)_5]$ compounds influences the excitation paths of the Eu(III) excited levels.

Figure 7 shows the emission spectra of the **1**, **2**, and **3** Eu(III) complexes recorded in the range of 530−720 nm, under excitation at the broad band of the picrate ligand at 370 nm, at

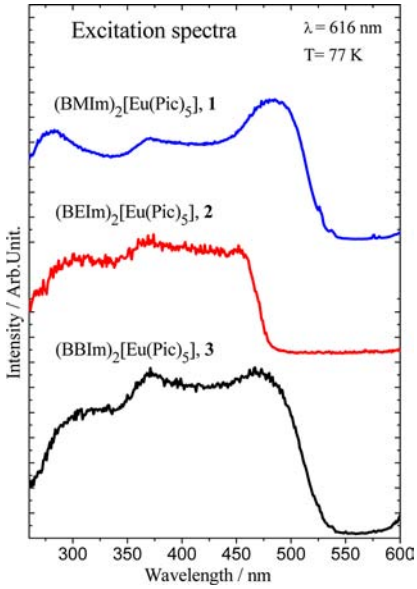

Figure 6. Excitation spectra of complexes **1**, **2**, and **3** recorded from 250 nm to 585 nm at 77 K with excitation monitored on hypersensitive $^5D_0 \rightarrow {}^7F_2$ transition at ~616 nm.

77 K. It presents narrow emission bands from the $^5D_0 \rightarrow {}^7F_J$ transitions (where $J = 0-4$) dominated by the hypersensitive $^5D_0 \rightarrow {}^7F_2$ transition at 616 nm. The presence of the $^5D_0 \rightarrow {}^7F_0$ transition indicates that the Eu(III) ion is located in a symmetry site of the type C_s, C_n, or C_{nv}. Since the $^5D_0 \rightarrow {}^7F_1$ emission is almost insensitive to changes in the chemical environment, it is primarily magnetic dipole by character, while the $^5D_0 \rightarrow {}^7F_2$ emission is essentially forced electric dipole in character, and its intensity is very sensitive to the ligand field interaction.[50]

It is noteworthy that the spectra of the Eu(III) complexes recorded at room temperature and low temperature showed similar profiles. However, the emission spectra at room temperature (not shown) are less resolved, compared to the spectra obtained at liquid nitrogen temperature (77 K).

Another feature in the photoluminescence data of the pentakis complexes is that the emission spectra of all Eu(III) complexes do not exhibit the broad phosphorescence band of the Pic ligands that is observed in the Gd(III) complexes (see Figure 7), indicating energy transfer ligand-lanthanide ion.

dx.doi.org/10.1021/ic301776n | Inorg. Chem. 2012, 51, 12867−12878

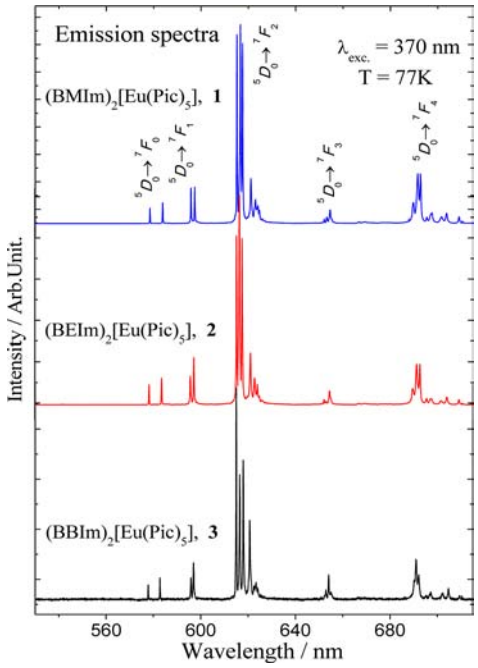

Figure 7. Emission spectra of complexes **1**, **2**, and **3** at 77 K recorded from 500 nm to 720 nm under excitation at 370 nm.

The experimental intensity parameters values of Ω_2 and Ω_4 were calculated and compared with theoretical intensity parameters Ω_λ (λ = 2, 4, and 6) obtained using the spherical atomic coordinates from the Sparkle/PM3 coordination polyhedron. The results are presented in Table 6. The charge factors (g) and the ligating ion polarizability (α), which are used in the calculations of γ_p^t and Γ_p^t, respectively, were adjusted using a nonlinear minimization of a four-dimensional response surface to minimize the error between the experimental and theoretical values of the Ω_2 and Ω_4 parameters. The procedure is described in detail in the literature.[51] The values of charge factors (g) and the ligating ion polarizability (α) are given in Table 3. According to the theory, the value of the intensity parameter Ω_2 is most influenced by small angular changes in the local geometry. This effect, together with changes in ligating atom polarizability (α), has been used to rationalize the fact that certain $4f$–$4f$ transitions are hypersensitive to changes in the chemical environment.[52] The fact that the Ω_2 and Ω_4 parameters (both experimental and theoretical) have comparable values is an indication that the coordination geometry around the Eu(III) ion presents a low symmetry that originates from a distortion of a high-symmetry coordination geometry containing a center of inversion, according to the model developed in ref 53.

Table 6. Calculated and Experimental Values of Intensity Parameters (R_{02} and Ω_λ), Radiative (A_{rad}) and Nonradiative (A_{nrad}) Rates, Lifetimes (τ), Emission Quantum Efficiencies (η), and Emission Quantum Yields (q) of the $^5D_0$ Emitting Level Determined for Complexes 1, 2, and 3

	1		2		3	
optical data	exp.	calc.	exp.	calc.	exp.	calc.
R_{02}	0.018		0.009		0.011	
Ω_2 ($\times 10^{-20}$ cm^2)	15.1	13.6	12.0	15.0	9.6	11.9
Ω_4 ($\times 10^{-20}$ cm^2)	13.9	8.6	10.3	8.8	9.2	10.3
Ω_6 ($\times 10^{-20}$ cm^2)		0.3		0.2		0.1
A_{rad} (s^{-1})	645	591.3	691	636.5	614	565.8
A_{nrad} (s^{-1})	797	851.7	1159	1215.3	603	652.2
τ (ms)	0.521		0.628		0.821	
η (%)	45.0	41.0	37.0	34.3	51.0	46.4
q (%)		38.2		27.7		10.8

Table 6 also presents the theoretical and experimental values of the radiative and nonradiative rates of spontaneous emission (A_{rad} and A_{nrad}, respectively), emission efficiency (η), emission quantum yield (q, theoretical), and experimental lifetimes (τ) for the $(BMIm)_2[Eu(Pic)_5]$ (**1**), $(BEIm)_2[Eu(Pic)_5]$ (**2**), and $(BBIm)_2[Eu(Pic)_5]$ (**3**) complexes.

The lifetime of the emitting state $^5D_0$ (τ), and the nonradiative (A_{nrad}) and radiative (A_{rad}) rates, are related through

$$A_{tot} = \frac{1}{\tau} = A_{rad} + A_{nrad} \quad (13)$$

where the A_{rad} rate was obtained by summing over the radiative rates $A_{0\lambda}$ for each $^5D_0 \rightarrow {}^7F_\lambda$ transition ($A_{rad} = \sum_\lambda A_{0\lambda}$). The definition of the emission quantum efficiency (η) of the emitting $^5D_0$ level, used here, is

$$\eta = \frac{A_{rad}}{A_{rad} + A_{nrad}} \quad (14)$$

The theoretical radiative and nonradiative rates, and quantum efficiencies, are also in good agreement with the experimental values. The value of the emission quantum efficiency, in principle, should not be dependent on the T_1 position. Thus, the η behavior shown in Table 6 reflects vibronic couplings, through A_{nrad}, with the ligands, influenced by the countercations. A detailed investigation of this point is beyond the scope of the present work.

Table 6 presents also the R_{02} intensity parameter, which is the ratio between the intensities of the $^5D_0 \rightarrow {}^7F_0$ and $^5D_0 \rightarrow {}^7F_2$ transitions. The R_{02} parameter may give information on the J-mixing effect associated with the $^5D_0 \rightarrow {}^7F_0$ transition, as previously described.[5,54] In this case, this effect is mainly due to the mixing between the $^7F_2$ manifold and the $^7F_0$ level though the rank-two components of the ligand field. The R_{02} value for compound **2** is one order of magnitude smaller than for complexes **1** and **3**, suggesting that the J-mixing effect is much smaller in this complex, taking into consideration that, in the three complexes, the $^5D_0 \rightarrow {}^7F_0$ transition is allowed by symmetry.

The experimental and theoretical values of the triplet states of the **1**, **2**, and **3** complexes are in very satisfactory agreement. The triplet state of the complex with the $BMIm^+$ countercation (19 512 cm^{-1}) is above the $^5D_1$ (19 070 cm^{-1}) state, and according to the selection rules mentioned above, the energy transfer $T_1 \rightarrow {}^5D_1$ by the exchange mechanism is much more favored than in the cases of the complexes with the $BEIm^+$ countercation, **2** (T_1 at 19 065 cm^{-1}) and the $BBIm^+$ countercation, **3** (T_1 at 18 504 cm^{-1}). Particularly, in the latter case, energy back-transfer $^5D_1 \rightarrow T_1$ is expected to be more operative in the transfer process balance. On the other hand, an opposite behavior should occur for the less-operative $T_1 \rightarrow {}^5D_0$ transfer process (balanced by the back-transfer rate) by the multipolar mechanism, together with the J-mixing effect. The transfer rates corresponding to this process are, at the most, on the order of 10^6 s^{-1}, which is the order of magnitude of the nonradiative decay rates for $^5D_1 \rightarrow {}^5D_0$ in coordination compounds. These facts explain both the decrease of the emission quantum yield and the increase of the $^5D_0$ lifetime in going from complex **1** to complex **3** (see Table 6).

dx.doi.org/10.1021/ic301776n | Inorg. Chem. 2012, 51, 12867−12878

From a schematic energy level diagram shown in Figure 8, the resonance conditions may be represented. For the three Eu complexes studied, the singlet levels are below the $^5D_4$ europium excited state.

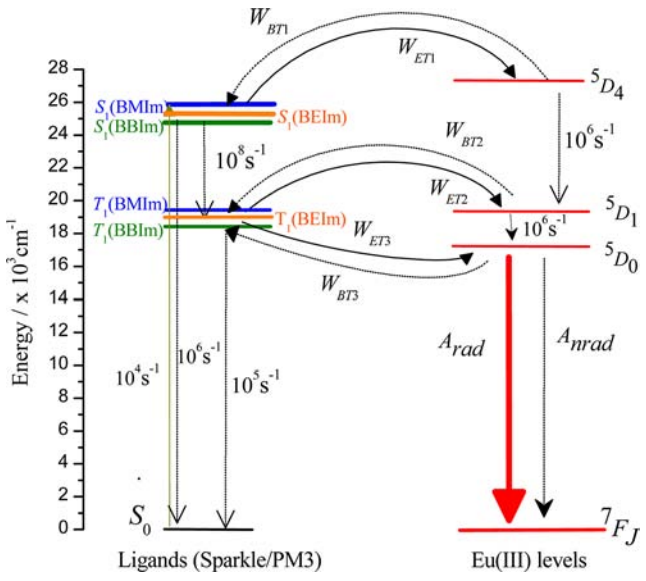

Figure 8. Energy level diagram for complexes **1**, **2**, and **3**, showing the most probable channel for the intramolecular energy transfer process.

From the luminescence decay curves (Figure 9), we have determined the lifetime values (τ) of the emitting $^5D_0$ level at

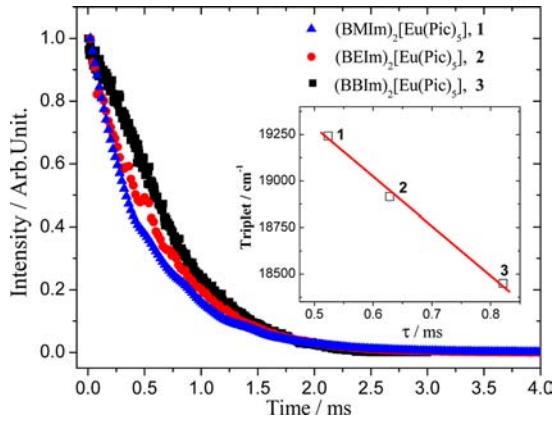

Figure 9. Decay luminescence curves of complexes **1**, **2**, and **3** recorded at 77 K monitored with excitation at 370 nm and emission at 616 nm. The inset shows the relation between the lifetimes of the $^5D_0$ level and the T_1 position.

room temperature (300 K), monitored with excitation at 370 nm and emission at 616 nm. These curves were fitted with a monoexponential curve with lifetime values of 0.523, 0.628, and 0.821 ms for the Eu(III) complexes with $BMIm^+$, $BEIm^+$, and $BBIm^+$ countercations, respectively. A decreasing linear behavior is observed when a triplet versus lifetime graphic is drawn (shown in the insert of Figure 9), demonstrating the influence of the countercation in the luminescence process.

Despite the same composition of the first coordination sphere, the luminescence properties of these compounds are significantly different. The existence of an additional path for fine-tuning of the luminescence properties can be optimized by changing the C^+ countercation, and this small change produces a considerable modification in the electronic structure of the organic part of the compounds.[55,56] Since this influences the structure of the complex, it affects the position of the triplet state and, as a consequence, the emission quantum yield, making $(C)_2[Ln(L)_5]$-type compounds very interesting materials both for theoretical studies and practical applications for designing new LCMDs.[57]

5. CONCLUSIONS

In this study, we present the first $(LnL_5)^{2-}$ pentakis complexes with a picrate ligand, and we show that the BMIm, BEIm, and BBIm countercations have a significant influence on their optical properties. An additional tuning of the optical parameters of $(C)_2[Eu(Pic)_5]$-type complexes may be achieved by an appropriate choice of the C^+ countercation. The theoretical emission quantum yields are 38.2, 27.7, and 10.8% for the $(BMIm)_2[Eu(Pic)_5]$ (**1**), $(BEIm)_2[Eu(Pic)_5]$ (**2**), and $(BBIm)_2[Eu(Pic)_5]$ (**3**) complexes, respectively. The triplet state of the complex with the $BMIm^+$ countercation (19 512 cm^{-1}) is above the $^5D_1$ state (19 070 cm^{-1}), and the energy transfer $T_1 \rightarrow D_1$ by the exchange mechanism is much more favored than in the cases of the complexes with the $BEIm^+$ countercation (T_1 at 19 065 cm^{-1}) and the $BBIm^+$ countercation (T_1 at 18 504 cm^{-1}). On the other hand, energy back-transfer increases in this same direction. These facts explain the trend observed in the calculated emission quantum yields. A decreasing linear behavior was observed when a plot of triplet versus lifetime is drawn, demonstrating the influence of the countercation in the luminescence process.

■ ASSOCIATED CONTENT

Ⓢ Supporting Information

The deposition numbers CCDC 888983 and 888984 contain the supplementary crystallographic data for $(BEIm)_2[Eu(Pic)_5]$ (**2**) and $(BBIm)_2[Eu(Pic)_5]$ (**3**), respectively. These data can be obtained free of charge from The Cambridge Crystallographic Data Centre via www.ccdc.cam.ac.uk/data_request/cif. The synthesis and characterization of the bromide and picrate ionic liquids, which have been published previously, also are provided. Absorption spectra of $(BMIm)_2[Eu(Pic)_5]$ (**1**) and **3** complexes were recorded in acetonitrile (experimental) and calculated in overlay mode (theoretical). This material is available free of charge via the Internet at http://pubs.acs.org.

■ AUTHOR INFORMATION

Corresponding Author

* Tel.: +55 11 30913847. Fax: +55 11 38155579. E-mail: hefbrito@iq.usp.br.

Present Address

⊥Departamento de Química e Biologia, Instituto Federal de Educação, Ciência e Tecnologia do Espirito Santo, Vitória-ES, 29040-780, Brazil.

Notes

The authors declare no competing financial interest.

■ ACKNOWLEDGMENTS

The authors express sincere thanks to Laboratory of Photonic Materials (UNESP-Araraquara)—particularly, Dr. Sidney J. L. Ribeiro and Dr. Maurício Caiut—for some luminescence measurements. We also thank CNPq-RENAMI, CNPq-FAPEMIG, FAPITEC-SE, INAMI, and LabCri (X-ray diffraction

studies DF/ICEx-UFMG)—particularly, Professor Nilvado L. Speziali—for the measurements and for the support with the X-ray facilities.

REFERENCES

(1) *Lanthanide Probes in Life, Chemical, and Earth Sciences: Theory and Practice*; Bunzli, J.-C. G., Choppin, G. R., Eds.; Elsevier: Amsterdam, 1989; Chapter 7.
(2) Pietraszkiewicz, M.; Karpiuk, J.; Rout, A. K. *Pure Appl. Chem.* **1993**, *65*, 563−566.
(3) Brito, H. F.; Malta, O. L.; Felinto, M. C. F. C.; Teotonio, E. E. S. The Chemistry of Metal Enolates. In *Luminescence Phenomena Involving Metal Enolates*, Vol. *1*; Zabicky, J., Ed.; John Wiley & Sons, Ltd.: Chichester, U.K., 2009; Chapter 3, pp 131−184.
(4) Gawryszewska, P.; Sokolnichi, J.; Legendziewicz, J. *Coord. Chem. Rev.* **2005**, *249*, 2489−2509.
(5) Sabbatini, N.; Guardigli, M.; Lehn, J. M. *Coord. Chem. Rev.* **1993**, *123*, 201−228.
(6) Carnall, W. T.; Gruen, D. M.; McBeth, R. L. *J. Phys. Chem.* **1962**, *66*, 2159−2165.
(7) Carnall, W. T. *J. Phys. Chem.* **1963**, *67*, 1206−1211.
(8) Carnall, W. T.; Fields, P. R.; Wybourne, B. G. *J. Chem. Phys.* **1965**, *42*, 3797−3806.
(9) Kim, Y. H.; Baek, N. S.; Kim, H. K. *Chem. Phys. Chem* **2006**, *7*, 213−221.
(10) Teotonio, E. E. S.; Espínola, J. G. P.; Oliveira, S. F.; Farias, D. L.; Malta, O. L; Brito, H. F. *Polyhedron* **2002**, *21* (18), 1837−1844.
(11) Malta, O. L; Brito, H. F.; Meneses, J. F. S.; Donega, C. F., Jr; Farias, F. S. *Chem. Phys. Lett.* **1998**, *282*, 233−238.
(12) Saleh, M. I.; Kusrini, E.; Mohd Sarjidan, M. A.; Abd. Majid, W. H. *Spectrochim. Acta, Part A* **2011**, *78*, 52−58.
(13) Freire, R. O.; Rocha, G. B.; Simas, A. M. *Inorg. Chem.* **2005**, *44*, 3299−3310.
(14) Freire, R. O.; Rocha, G. B.; Simas, A. M. *J. Braz. Chem. Soc.* **2009**, *20*, 1638−1645.
(15) Freire, R. O.; Simas, A. M. *J. Chem. Theory Comput.* **2010**, *6*, 2019−2023.
(16) Mesquita, M. E.; Silva, F. R. G.; Albuquerque, R. Q.; Freire, R. O.; da Conceição, E. C.; Júnior, N. B. C.; da Silva, J. E. C.; de Sá, G. F. *J. Alloys Compd.* **2004**, *366*, 124−131.
(17) Mesquita, M. E.; Júnior, S. A.; Silva, F. R. G.; dos Santos, M. A. C.; Freire, R. O.; Júnior, N. B. C.; de Sá, G. F. *J. Alloys Compd.* **2004**, *374*, 320−324.
(18) Freire, R. O.; Rodrigues, M. O.; Silva, F. R. G.; Júnior, N. B. C.; Mesquita, M. E. *J. Mol. Model.* **2005**, *12*, 16−23.
(19) Binnemans, K. In *Rare Earth Beta-Diketonates*; Gschneidner K. A., Jr., Bunzli, J. C.-G., Pecharsky, V. K., Eds.; Handbook on the Physics and Chemistry of Rare Earths, Vol. *35*; Elsevier: Amsterdam, 2004; pp 107−272.
(20) Nockemann, P.; Beurer, E.; Driesen, K.; Van Deun, R.; Van Hecke, K.; Van Meervelt, L.; Binnemans, K. *Chem. Commun.* **2005**, 4354−4356.
(21) Goossens, K.; Nockemann, P.; Driesen, K.; Goderis, B.; Gorller-Walrand, C.; Van Hecke, K.; Van Meervelt, L.; Pouzet, E.; Binnemans, K.; Cardinaels, T. *Chem. Mater.* **2008**, *20*, 157−168.
(22) Lunstroot, K.; Driesen, K.; Nockemann, P.; Van Hecke, K.; Van Meervelt, L.; Gorller-Walrand, C.; Binnemans, K.; Bellayer, S.; Viau, L.; Bideau, J. L.; Vioux, A. *Dalton Trans.* **2009**, 298−306.
(23) Holbrey, J. D.; Seddon, K. R. *Clean Prod. Process.* **1999**, *1*, 223−236.
(24) Wasserscheid, P.; Keim, W. *Angew. Chem., Int. Ed.* **2000**, *39*, 3772−3789.
(25) Welton, T. *Coord. Chem. Rev.* **2004**, *248*, 2459−2477.
(26) Ridley, J. E.; Zerner, M. C. *Theor. Chim. Acta* **1976**, *42*, 223−236.
(27) Ananias, D.; Kostova, M.; Paz, F. A. A.; Neto, A. N. C.; De Moura, R. T., Jr.; Malta, O. L.; Carlos, L. D.; Rocha, J. *J. Am. Chem. Soc.* **2009**, *131* (24), 8620−8626.
(28) Harrowfield, J. M.; Lu, W.; Skelton, B. W.; White, A. H. *Aust. J. Chem.* **1994**, *47*, 321−337.
(29) CRYSALISPRO, Version 1.171.34.34 (release 05-01-2010 CrysAlis171.NET); Oxford Diffraction, Ltd.: Wembly, Middlesex, U.K.
(30) Sheldrick, G. M. *Acta Crystallogr., Sect. A: Found. Crystallogr.* **2008**, *64*, 112−122.
(31) Farrugia, L. J. *J. Appl. Crystallogr.* **1999**, *32*, 837−838.
(32) Spek, A. L. *Acta Crystallogr., Sect. D: Biol. Crystallogr.* **2009**, *D65*, 148−155.
(33) MOPAC2009, Version 10.060W; Stewart, J. J. P., Ed.; Stewart Computational Chemistry (SCC): Colorado Springs, CO, 2009.
(34) Zerner, M. C.; Loew, G. H.; Kirchner, R. F.; Mueller-Westerhoff, U. T. *J. Am. Chem. Soc.* **1980**, *102*, 589−599.
(35) Zerner, M. C. *ZINDO Manual*; University of Florida: Gainesville, FL, No. 32611-8435, QTP, 1990.
(36) Judd, B. R. *Phys. Rev.* **1962**, *127*, 750−761.
(37) Ofelt, G. S. *J. Chem. Phys.* **1962**, *37*, 511−520.
(38) Malta, O. L.; Ribeiro, S. J. L.; Faucher, M.; Porcher, P. *J. Phys. Chem. Solids* **1991**, *52*, 587−596.
(39) Santos, E. R.; dos; Freire, R. O.; Costa, N. B., Jr; Paz, A. F. A.; Simone, C. A.; Júnior, S. A.; Araújo, A. A. S.; Nunes, L. A. O.; Mesquita, M. E.; Rodrigues, M. O. *J. Phys. Chem. A* **2010**, *114*, 7928−7936.
(40) de Sá, G. F.; Malta, O. L.; Donega, C. M.; Simas, A. M.; Longo, R. L.; Santa-Cruz, P. A.; Silva, E. F., Jr. *Coord. Chem. Rev.* **2000**, *196*, 165−195.
(41) Malta, O. L.; Silva, F. R. G. *Spectrochim Acta, Part A* **1998**, *54*, 1593−1599.
(42) Malta, O. L.; Silva, F. R. G.; Longo, R. *Chem. Phys. Lett.* **1999**, *307*, 518−526.
(43) Malta, O. L. *J. Non-Cryst. Phys.* **2008**, *354*, 4770−4776.
(44) Faustino, W. M.; Malta, O. L.; de Sá, G. F. *J. Chem. Phys.* **2005**, *122*, 4770−4776.
(45) Geary, W. J. *Coord. Chem. Rev.* **1971**, *7*, 81−122.
(46) Guo, Y.-L.; Wang, Y.-W.; Liu, W.-S.; Dou, W.; Zhong, X. *Spectrochim. Acta, Part A* **2007**, *67*, 624−627.
(47) Makovicky, E.; Balic-Zunic, T. *Acta Crystallogr., Sect. B: Struct. Sci.* **1996**, *B52*, 78−81.
(48) Balic-Zunic, T.; Vickovic, I. *J. Appl. Crystallogr.* **1996**, *29*, 305−306.
(49) Vologzhanina, A. V.; Pushkin, D. V.; Serezhkin, V. N. *Acta Crystallogr., Sect. B: Struct. Sci.* **2006**, *B62*, 754−760.
(50) Raj, D. B. A.; Biju, S.; Reddy, M. L. P. *Inorg. Chem.* **2008**, *47*, 8091−8100.
(51) Rodrigues, M. O.; Júnior, N. B. C.; Simone, C. A.; Araujo, A. A. S.; Brito-Silva, A. M.; Paz, F. A. A.; Mesquita, M. E.; Júnior, S. A.; Freire, R. O. *J. Phys. Chem. B* **2008**, *112*, 4204−4212.
(52) Malta, O. L. *Mol. Phys.* **1981**, *42*, 65−72.
(53) Sá Ferreira, R. A.; Nobre, S. S.; Granadeiro, C. M.; Nogueira, H. I. S.; Carlos, L. D; Malta, O. L. *J. Lumin.* **2006**, *121*, 561−567.
(54) Steemers, F. J.; Verboon, W.; Reinhoudt, D. N.; Vander Tol, E. B.; Verhoeven, J. W. *J. Am. Chem. Soc.* **1995**, *117*, 9408−9414.
(55) Mech, A.; Karbowiak, M.; Gorller-Walrand, C; Deun, R. V. *J. Alloys Compd.* **2008**, *451*, 215−219.
(56) Bruno, S. M.; Ferreira, R. A. S.; Paz, F. A. A.; Carlos, L. D.; Pillinger, M.; Ribeiro-Claro, P.; Gonçalves, I. S. *Inorg. Chem.* **2009**, *48*, 4882−4895.
(57) Bettinelli, M.; Speghini, A.; Piccinelli, F.; Neto, A. N. C.; Malta, O. L. *J. Lumin.* **2011**, *131*, 1026−1028.